

Large magneto-optic enhancement in ultra-thin liquid-phase-epitaxy iron garnet films

Miguel Levy, A. Chakravarty, H.-C. Huang, and R. M. Osgood Jr.

Citation: [Applied Physics Letters](#) **107**, 011104 (2015); doi: 10.1063/1.4926409

View online: <http://dx.doi.org/10.1063/1.4926409>

View Table of Contents: <http://scitation.aip.org/content/aip/journal/apl/107/1?ver=pdfcov>

Published by the [AIP Publishing](#)

Articles you may be interested in

[Plasmon resonance enhancement of Faraday rotation of liquid phase epitaxy grown garnet films populated with gold nanoparticles on the film surfaces](#)

J. Appl. Phys. **115**, 17A932 (2014); 10.1063/1.4866845

[Deposition of gold nanoparticles on liquid phase epitaxy grown garnet films and Faraday rotation enhancement](#)

J. Appl. Phys. **113**, 17A929 (2013); 10.1063/1.4799250

[Comment on "The role of Bi³⁺ ions in magneto-optic Ce and Bi comodified epitaxial iron garnet films" \[*Appl. Phys. Lett.* **97**, 161901 \(2010\)\]](#)

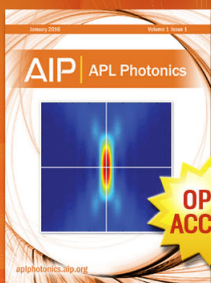
Appl. Phys. Lett. **99**, 126101 (2011); 10.1063/1.3610452

[Development of liquid phase epitaxy-grown \(Bi, Gd, Lu\)-substituted thin-film iron garnets](#)

J. Appl. Phys. **99**, 08M702 (2006); 10.1063/1.2164439

[Growth effects \(rotation rate\) on the characteristics of bismuth substituted lutetium iron garnets](#)

J. Appl. Phys. **95**, 6885 (2004); 10.1063/1.1669345



Launching in 2016!

The future of applied photonics research is here

OPEN
ACCESS

AIP | APL
Photonics

Large magneto-optic enhancement in ultra-thin liquid-phase-epitaxy iron garnet films

Miguel Levy,¹ A. Chakravarty,¹ H.-C. Huang,² and R. M. Osgood, Jr.³

¹Physics Department, Michigan Technological University, Houghton, Michigan 49931, USA

²Department of Electrical Engineering, Columbia University, New York, New York 10027, USA

³Applied Physics and Applied Mathematics, Columbia University, New York, New York 10027, USA

(Received 11 May 2015; accepted 24 June 2015; published online 6 July 2015)

Significant departures from bulk-like magneto-optic behavior are found in ultra-thin bismuth-substituted iron-garnet films grown by liquid-phase-epitaxy. These changes are due, at least in part, to geometrical factors and not to departures from bulk-composition in the transient layer at the film-substrate interface. A monotonic increase in specific Faraday rotation with reduced thickness is the signature feature of the observed phenomena. These are traced to size-dependent modifications in the diamagnetic transition processes responsible for the Faraday rotation. These processes correspond to the electronic transitions from singlet 6S ground states to spin-orbit split excited states of the Fe^{3+} ions in the garnet. A measurable reduction in the corresponding ferrimagnetic resonance linewidths is found, thus pointing to an increase in electronic relaxation times and longer lived excitations at reduced thicknesses. These changes together with a shift in vibrational frequency of the Bi-O bonds in the garnet at reduced thicknesses result in greatly enhanced magneto-optical performance. These studies were conducted on epitaxial monocrystalline $Bi_{0.8}Gd_{0.2}Lu_2Fe_5O_{12}$ films.
 © 2015 AIP Publishing LLC. [<http://dx.doi.org/10.1063/1.4926409>]

Numerous studies have been reported in the literature over the years on the magneto-optic properties of magnetic garnet films. These studies have been spurred by the central role played by magneto-optic non-reciprocity in technologically important optical devices such as isolators and circulators.^{1–15} Film-growth processes and elemental substitutions in these materials have been extensively investigated.^{4,7–9,12,14–16} Enhancing the specific Faraday rotation and reducing optical absorption losses are strong motivators to improve the optical performance of nonreciprocal devices. Early on, magnetic memory applications of iron garnets (bubble memory) also played a role in the development of better materials.¹³ The ultra-low spin-wave propagation damping in yttrium iron garnets is also spurring interest in thin films of these materials for spintronic and magnonic applications.¹⁷

Here, our interest is to examine dimensional effects in the magneto-optic response of sub-100-nm-thick liquid-phase-epitaxially (LPE)-grown monocrystalline films. Our primary investigation is to study the Faraday rotation and circular dichroism in this magnetic garnet system. Raman spectroscopy and Rutherford backscattering analysis (RBS) are also used to supplement our investigation.

The origins of Faraday rotation in magnetic garnet media are well addressed by Wittekoek and co-workers,⁸ Dionne,¹⁸ Allen and Dionne,¹⁹ and Hansteen *et al.*²⁰ Methods such as bismuth- and cerium-substitution in rare-earth iron garnets have been found to enhance the specific Faraday rotation in these material systems and are already discussed in numerous publications.^{4,8,14,15,18,20,21} Faraday rotation enhancement through photon trapping in magneto-photon crystal defects has also been investigated.^{22–25}

Prior work on dimensional effects in ultrathin magneto-optic garnet films has revealed changes in specific Faraday

rotation.²¹ No clear-cut enhancement in gyrotropic response has been reported and the effect has been ascribed to a transition between ferrimagnetic phases. Sputter-deposited films of various thicknesses were used in those studies. Among the key differences with the work reported here are that we analyze monocrystalline LPE-grown films rather than polycrystalline sputter-deposited ones, that we find a monotonic increase in specific Faraday rotation for sub-100-nm-thick films, and monotonic changes in magnetic circular dichroism (MCD), thus pointing to longer-lived electronic excitations in the absorption bands responsible for the Faraday rotation at reduced thicknesses. These are exciting results that indicate that phase-pure garnet can have its Faraday rotation enhanced by some intrinsic mechanism that has not been discovered in decades of excellent research.

Samples of $Bi_{0.8}Gd_{0.2}Lu_2Fe_5O_{12}$ are used in our investigation. These films are grown by liquid-phase-epitaxy on (100) gadolinium gallium garnet ($Gd_3Ga_5O_{12}$) substrates (GGG). They exhibit planar magnetic anisotropy and an extrapolated perpendicular saturating field similar to their saturation magnetization of $4\pi M_s \approx 1800G$. Growth conditions are stable, at a constant temperature to within $0.5^\circ C$ and a constant substrate rotation rate in the melt.²⁶ The film composition chosen for our samples yields lattice-parameter matching with that of the substrate to within $\pm 0.001 \text{ \AA}$. We should point out that since our main intention was to study dimensional effects on the magneto-optic response all the samples used in these investigations are obtained from the same original wafer by a wet-etch thin-down process.

A total of 15 $Bi_{0.8}Gd_{0.2}Lu_2Fe_5O_{12}$ films ranging in thickness from 19 nm to $2.72 \mu m$ were studied. The samples were prepared by sequential etching in an ortho-phosphoric acid bath with a slow-rotation rate to ensure uniform thickness. In order to minimize surface roughness, etch rates were

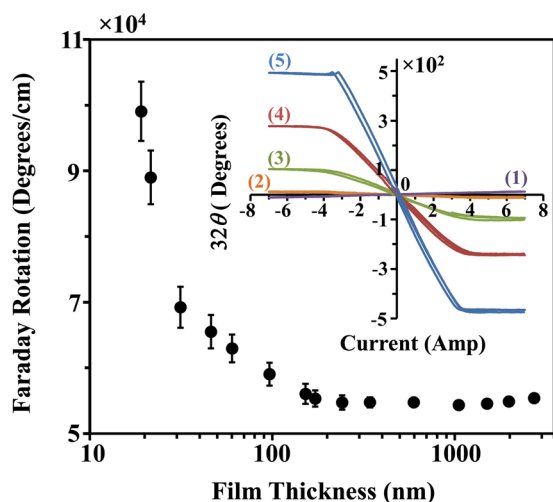


FIG. 1. Specific Faraday rotation θ versus film thickness for $\text{Bi}_{0.8}\text{Gd}_{0.2}\text{Lu}_2\text{Fe}_5\text{O}_{12}$ films (the substrate contribution has been folded out in these data) at 532 nm wavelength. Inset: Faraday rotation hysteresis loops measured on the $\text{Bi}_{0.8}\text{Gd}_{0.2}\text{Lu}_2\text{Fe}_5\text{O}_{12}$ films for different thicknesses and on the GGG substrate: (1) substrate, (2) 60 nm, (3) 590 nm, (4) 1520 nm, and (5) 2720 nm. The magnetic field is expressed in terms of the current in the electromagnet.

controlled by adjusting the temperature of the acid bath, from 85 °C to 120 °C. Surface roughness was examined by atomic force microscopy on 4 samples, ranging in thickness from 21.5 nm (1.3 nm mean surface roughness) to 343 nm (4.7 nm mean surface roughness). After etching, the samples were rinsed in de-ionized-water and their thickness measured in a V-Vase ellipsometer in reflection. Thickness uniformity was verified by probing different points of the sample surface. Sample thickness measurement via transmission-electron microscopy was also used to obtain an independent thickness determination on several of these samples. Small differences in thickness determination were found between the two techniques ($\sim 8\%$ for the thinnest samples), but the monotonic specific Faraday-rotation enhancement trend seen in Fig. 1 for sub-100 nm-thick films remained unaffected.

Light from a 532 nm-wavelength CW diode-pumped-solid-state laser source was used to probe the Faraday rotation. After passing through a polarizer, the light impinged at normal incidence on samples placed between bored pole pieces of an electromagnet, then through a rotating

Glan-Thompson analyzer, and was detected by a silicon photo-receiver.¹⁰ This sinusoidal signal was fed to a lock-in amplifier after passing through a frequency multiplier that synchronized it with the reference signal. The difference in phase between these two signals is a measure of the Faraday rotation induced by the sample. A U-shaped LED-plus-photoelectric sensor provided the reference signal from slots cut out in an aluminum wheel mounted on the same hollow-shaft-motor housing the Glan-Thompson cube. The wheel was equipped with 32 equidistantly spaced slots at the rim, so that a 360° revolution around its axis delivered 32 reference pulses to the lock-in amplifier. The net effect of this arrangement was to amplify by that same factor the phase shift read by the phase monitor of the lock-in upon a Faraday rotation of the incoming linearly polarized light. This provided enough accuracy in our Faraday rotation measurements (better than 0.001°) to comfortably probe sub-hundred-nm-thick films.

Faraday-rotation hysteresis loops were recorded for each sample. Field scans up to a maximum magnetic field of 2700 Oe at 19.3 Oe scan field-steps were recorded and the Faraday rotation at saturation was chosen to characterize the response of each film. Since the films were grown on paramagnetic GGG, we had to subtract out the substrate's response from the overall Faraday rotation signal. Hysteresis loop measurements were thus carried out on bare substrate samples for calibration purposes. Representative hysteresis loops are plotted as an inset to Fig. 1.

Magnetic circular dichroism measurements at room temperature were performed in a V-Vase ellipsometer under a 1.3 T magnetic field to analyze the absorption bands responsible for the Faraday rotation in these iron-garnet films (Fig. 2). Each sample was placed in an aluminum mount holding two strong neodymium magnet rings 10 mm apart, configured to magnetize the sample in the normal direction. Absorption measurements for both right- and left-circularly polarized light were done in the 260 to 800 nm wavelength range. A bare 1 mm-thick GGG substrate was also analyzed to fold out the substrate contribution from that of the film-plus-substrate samples. Right and left circularly polarized light were sent through the samples and transmission spectra were recorded. Transmission spectra were corrected to account for reflections by normalizing to the substrate transmittance. These data were used to calculate absorption

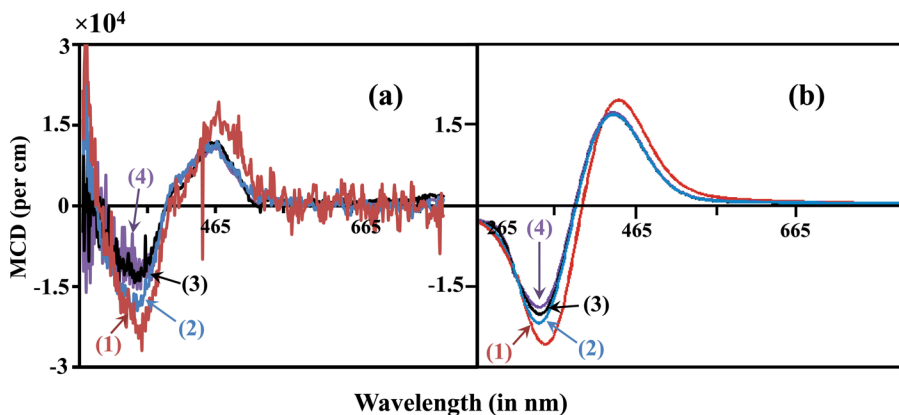


FIG. 2. Magnetic circular dichroism on four $\text{Bi}_{0.8}\text{Gd}_{0.2}\text{Lu}_2\text{Fe}_5\text{O}_{12}$ films of different thicknesses: (a) Experimental results. (b) Theoretical analysis calculated from the permittivity tensors for iron garnets as explained in the text. The curves correspond to the following film thicknesses: (1) 19 nm, (2) 46 nm, (3) 95 nm, and (4) 153 nm.

coefficients throughout the whole wavelength range. Magnetic circular dichroism is defined here as the difference in the absorption coefficients between the two circular polarizations at each wavelength.

Since magnetic circular dichroism in the absorption bands provides an independent determination of Faraday rotation at the 532 nm probe wavelength through the Kramers-Kronig relations, these measurements were also used to calculate the specific Faraday response as a function of sample thickness. This analysis yielded independent confirmation of the growing trend in specific Faraday rotation below 100 nm seen in Fig. 1. Additionally, our MCD measurements, in conjunction with Kramers-Kronig, reveal a Faraday rotation in the bulk of 830°/cm at 1550 nm wavelength.

Selected samples were further investigated by confocal micro-Raman spectroscopy to explore any compositional difference and/or strain at the interface. The micro-Raman measurements were performed in a backscattered geometry at room ambient conditions. The excitation wavelength was 532 nm. An 1800 lines/mm grating was used to achieve a spectral resolution of $\sim 1.5 \text{ cm}^{-1}$. Lorentzian peak fitting was performed on the spectra between the range of 600–800 cm^{-1} to reveal the information of peak intensity and position.

Figure 1 shows the specific Faraday rotation per centimeter at saturation field for each film analyzed in this work. These data were extracted from the recorded hysteresis loops. It can be seen from this figure that the specific rotation grows steadily for films thinner than ~ 100 nm. Uncertainties in our data stem from a few sources of error. Frequency fluctuations in the lock-in amplifier's reference signal due to imperfect equidistance between the slots in the rotating wheel around the Glan-Thompson polarizer lead to $\pm 0.05^\circ$ variations in unnormalized Faraday rotation values. Similarly, there were these uncertainties in the ellipsometrically measured thickness, i.e., $\sim \pm 1$ nm.

An enhancement in the specific Faraday rotation at 532 nm can be traced back to a corresponding enhancement in magnetic circular dichroism in the absorption bands of the iron garnet.^{18–20} The real part of the dielectric permittivity at this wavelength (532 nm), and hence the difference in refractive indices between right- and left-circular polarizations, is a function of the magnetic circular dichroism at all other wavelengths. This is a consequence of the Kramers-Kronig relations.

Thus, following the formulation of Dionne and Allen for bismuth-substituted iron garnets,^{18,19} the magnetic circular dichroism at wavelength λ in the absorption bands is given by

$$\Delta\alpha = \frac{4\pi}{\lambda} \left(\frac{k\varepsilon_1' - n\varepsilon_1''}{n^2 + k^2} \right), \quad (1)$$

where n and k are the average real and imaginary parts of the refractive index (averaged over both circular polarizations), and the diamagnetic functions for the off-diagonal components of the permittivity tensor elements $\varepsilon_1 = \varepsilon_1' + i\varepsilon_1''$ are described by

$$\varepsilon_1(\omega) = \omega_p^2 \sum_{i=a,d} \sum_{\pm} \frac{f_{i\pm}}{2\omega_{i0}} \times \frac{\omega(\omega_{i0\pm}^2 - \omega^2 - \Gamma_i^2) + i\Gamma_i(\omega_{i0\pm}^2 + \omega^2 + \Gamma_i^2)}{[(\omega_{i0\pm}^2 - \omega^2 + \Gamma_i^2)^2 + 4\omega^2\Gamma_i^2]}. \quad (2)$$

The summation indices a and d refer to the octahedral- and tetrahedral-coordinated sub-lattices of the garnet, respectively; $\omega_p = \sqrt{\frac{4\pi N e^2}{m\varepsilon(\infty)}}$ is the plasma frequency, N is the density of electronic transition centers, $\varepsilon(\infty)$ is the dielectric permittivity at very large frequencies, e and m are the electron charge and mass; $f_{i\pm} = \pm(f_i/2)(1 \pm \Delta_i/\omega_{i0})$ are the oscillator strengths of the positive and negative circular-polarization-induced electronic transitions; ω_{i0} and Γ_i correspond, respectively, to the resonance frequency and half-linewidth of the transition from the ground state to the Fe^{3+} excited state that is spin-orbit split by $2\Delta_i$; and $\omega_{i0\pm} = \omega_{i0} \pm \Delta_i$.

Fits to this model show good agreement with the experimental MCD data and are displayed in Fig. 2. Suitably adjusted standard parameter-values found in the literature for Bi-substituted iron garnets are used for the thicker 153 nm film.^{18,19} In order to fit the data for the thinner samples, we explore variations in all the relevant parameters, $\omega_p^2 f_{i\pm}$, ω_{i0} , Δ_i , and Γ_i . Reductions in the half-linewidth Γ_d for the higher-energy tetrahedral sub-lattice-transition are found for the 95 nm-thick-film (19% reduction) and 46 nm-thick-film (39% reduction). A 2% reduction in the octahedral sub-lattice resonant frequency ω_{a0} together with an 11% reduction in the corresponding octahedral half-linewidth Γ_a reproduces the 19 nm-thick film MCD results. No significant departures in bulk Bi concentration through its effect on spin-orbit splitting or oscillator strength are detected. In summary, the model points to an enhancement in the lifetime of electronic excitations at reduced film thicknesses below ~ 100 nm.

Evidence of longer decay rates and lifetime enhancement in electronic transitions in nanoscale structures has been reported in another material system.²⁷ The occurrence of a sharp enhancement in excitation state lifetimes in that case has been attributed to surface effects. Further investigation of the surface contribution to the decay rate mechanism in our ultra-thin garnet films is planned.

Direct experimental confirmation on the composition of the films in the bulk region and the transient layer at the interface (with the GGG substrate) were obtained from Rutherford-backscattering data. Four samples of different thicknesses, ranging from 19 nm to 340 nm, all from the same LPE-grown wafer, were analyzed. The transient layer was modeled to contain Ga in addition to Bi, Lu, Fe, Gd, and oxygen, since the substrate composition is $\text{Gd}_3\text{Ga}_5\text{O}_{12}$. We assume that some of these elements diffuse into the film during growth. Only an average composition for the transient layer was sought. The bulk composition for the thickest of these films (340 nm) was found to be $\text{Bi}_{0.8}\text{Gd}_{0.2}\text{Lu}_{2.0}\text{Fe}_{4.5}\text{O}_{12}$ per formula unit (pfu), and for the thinnest (19 nm), $\text{Bi}_{0.7}\text{Gd}_{0.2}\text{Lu}_{2.0}\text{Fe}_{5.0}\text{O}_{12}$. The transient layer was measured

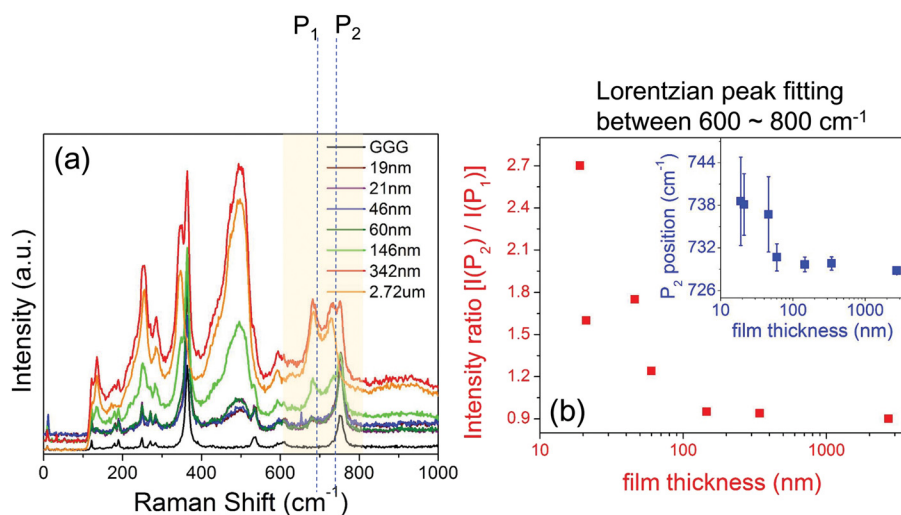


FIG. 3. (a) Raman shifts as a function of film thickness showing (b) enhancement in intensity ratio and shifts in relative peak position.

at 16 nm-thick for the thickest (340 nm) film with $\text{Bi}_{0.8}\text{Gd}_{0.2}\text{Lu}_{2.0}\text{Fe}_{5.0}\text{Ga}_{0.1}\text{O}_{12}$ pfu. An important feature of these data is that in none of the four samples analyzed was the average Bi content across the thickness (including the transient layer) found to exceed 0.8 pfu. This is noteworthy since it is mainly the addition of Bi that is known to enhance the specific Faraday rotation through composition changes. These results are consistent with our finding that average composition is not the main contributor to the enhancement we find in specific Faraday rotation at reduced thicknesses. However, these data do not rule out any effects arising from compositional gradients in the transient layer. It should be noted, however, that prior work (in the 1980s) found somewhat enriched levels of Bi in the transient layer as compared to the bulk of the film.²⁸

Finally, we have also conducted micro-Raman spectroscopy on several of our samples as a function of film thickness. The results are shown in Fig. 3(a). Note that the exposure time of the excitation on each film was optimized such that the obtained spectra can be vertically displaced for clarity. In particular, Lorentzian peak fitting was performed on the spectra between the wavenumber of 600–800 cm^{-1} to investigate the effects of film thickness on phonon modal activities. In this spectral range, Raman modes at $\sim 685 \text{ cm}^{-1}$ (denoted P_1) and $\sim 729 \text{ cm}^{-1}$ (denoted P_2), originating from the intrinsic $\text{Bi}_{0.8}\text{Gd}_{0.2}\text{Lu}_2\text{Fe}_5\text{O}_{12}$ film, and mode at $\sim 740 \text{ cm}^{-1}$, originating from the GGG substrate, were revealed, respectively. The peak intensity ratio of $I(P_2)/I(P_1)$ and the mode location of P_2 were further characterized and shown in Fig. 3(b). As seen in Fig. 3(b), these features show a similar trend of changes as compared to the Faraday rotation data in Fig. 1. Raman peak-ratio and peak-separation enhancement on selected pairs of Raman peaks are found for reduced film thickness (Fig. 3). It is possible that the surface and compositional gradients at the interface are playing a role in our observations and that these are affecting the vibrational modes and electronic relaxation times. These changes reflect variations in electronic polarizability through lattice modifications below $\sim 100 \text{ nm}$.

A particularly interesting feature of these Raman data is that the observed shifts occur in the Raman frequency range corresponding to the vibrational frequencies of bismuth-

oxygen dimers, as computed by density functional theory. This is calculated to be 718 cm^{-1} . Thus thickness reduction in these garnet films appears to affect these bond strengths and the corresponding magneto-optic response of the system.

The key finding from our Faraday rotation and transmission measurements is that the specific Faraday rotation increases monotonically as the $\text{Bi}_{0.8}\text{Gd}_{0.2}\text{Lu}_2\text{Fe}_5\text{O}_{12}$ film thickness is reduced below $\sim 100 \text{ nm}$. Enhancement in circular dichroism and absorbance over a broad wavelength range in the ultra-violet and visible are observed in the ultra-thin films. Our findings indicate that these effects and the corresponding enhancement in magneto-optic response in sub-100 nm LPE garnet films are linked to longer-lived electronic excitations in the diamagnetic transitions and modifications in the Bi-O vibrational frequencies, possibly due to surface effects and compositional gradients. These enhanced-response thin magneto-optic films may find potential application in nonreciprocal on-chip and spintronic devices.

This material is based upon work supported by the National Science Foundation under Grants Nos. 0856650 (M.L.) and 1302488 (R.M.O. and H.-C.H.). All films for this study were grown at Integrated Photonics, Inc., by V. J. Fratello. The authors thank V. J. Fratello for the LPE films, Owen P. Mills for help with the TEM analysis, Michael Chase for assembling the frequency multiplier, and Patrick Bowen for the AFM analysis. We thank G. Wang for the density functional theory calculations and R. Pandey for useful discussions. The authors also thank G. Malladi and H. Bakhru for the RBS measurements and analysis.

¹N. K. Dissanayake, M. Levy, A. A. Jalali, and V. J. Fratello, *Appl. Phys. Lett.* **96**(18), 181105 (2010).

²Z. Wu, M. Levy, V. J. Fratello, and A. M. Merzlikin, *Appl. Phys. Lett.* **96**(5), 051125 (2010).

³Y. Shoji, T. Mizumoto, H. Yokoi, I.-W. Hsieh, and R. M. Osgood, Jr., *Appl. Phys. Lett.* **92**(7), 071117 (2008).

⁴A. K. Zvezdin and V. A. Kotov, *Modern Magnetooptics and Magneto-optical Materials* (CRC Press, 1997).

⁵F. J. Rachford, M. Levy, R. M. Osgood, Jr., A. Kumar, and H. Bakhru, *J. Appl. Phys.* **87**(9), 6253 (2000).

⁶S. Geller, Proceedings of the International School of Physics “Enrico Fermi,” Course LXX, 1978.

⁷G. B. Scott, Proceedings of the International School of Physics “Enrico Fermi,” Course LXX, 1978.

- ⁸S. Wittekoek, T. J. A. Popma, J. M. Robertson, and P. F. Bongers, *Phys. Rev. B* **12**(7), 2777 (1975).
- ⁹S.-Y. Sung, X. Qi, and B. J. H. Stadler, *Appl. Phys. Lett.* **87**(12), 121111 (2005).
- ¹⁰J. F. Dillon, Proceedings of the International School of Physics “Enrico Fermi,” Course LXX, 1978.
- ¹¹S. H. Wemple, S. L. Blank, J. A. Seman, and W. A. Biolsi, *Phys. Rev. B* **9**(5), 2134 (1974).
- ¹²V. J. Fratello and R. Wolfe, *Handbook of Thin Films* (Academic Press, 2000), Vol. 4.
- ¹³K. Ando, N. Koshizuka, T. Okuda, and Y. Yokoyama, *Jpn. J. Appl. Phys.* **22**(10A), L618 (1983).
- ¹⁴H. A. Algra, J. M. Robertson, and H. Dötsch, *Appl. Phys.* **22**(2), 189 (1980).
- ¹⁵A. H. Eschenfelder, *Magnetic Bubble Technology* (Springer-Verlag, Berlin, 1980).
- ¹⁶P. Hansen, C.-P. Klages, J. Schuldt, and K. Witter, *Phys. Rev. B* **31**(9), 5858 (1985).
- ¹⁷M. Haidar, M. Ranjbar, M. Balinsky, R. K. Dumas, S. Khartsev, and J. Åkerman, *J. Appl. Phys.* **117**(17), 17D119 (2015).
- ¹⁸G. F. Dionne, *Magnetic Oxides* (Springer, 2009), p. 355.
- ¹⁹G. A. Allen and G. F. Dionne, *J. Appl. Phys.* **73**(10), 6130 (1993).
- ²⁰F. Hansteen, L. E. Helseth, T. H. Johansen, O. Hunderi, A. Kirilyuk, and T. Rasing, *Thin Solid Films* **455**, 429 (2004).
- ²¹V. Berzhansky, T. Mikhailova, A. Shaposhnikov, A. Prokopov, A. Karavainikov, V. Kotov, D. Balabanov, and V. Burkov, *Appl. Opt.* **52**(26), 6599 (2013).
- ²²M. Inoue, K. Arai, T. Fujii, and M. Abe, *J. Appl. Phys.* **83**(11), 6768 (1998).
- ²³M. J. Steel, M. Levy, and R. M. Osgood, *J. Lightwave Technol.* **18**(9), 1297 (2000).
- ²⁴S. Kahl and A. M. Grishin, *Phys. Rev. B* **71**(20), 205110 (2005).
- ²⁵M. Levy and R. Li, *Appl. Phys. Lett.* **89**(12), 121113 (2006).
- ²⁶V. J. Fratello, I. Mnushkina, S. J. Licht, and R. R. Abbott, *Magneto-Optical Materials for Photonics and Recording* (Proc. Mater. Res. Soc. Symp., 2005), Vol. 834, p. 229.
- ²⁷C. C. S. Chan, B. P. L. Reid, R. A. Taylor, Y. Zhuang, P. A. Shields, D. W. E. Allsopp, and W. Jia, *Appl. Phys. Lett.* **102**(11), 111906 (2013).
- ²⁸E. I. Filippov, *Sov. Phys. Tech. Phys.* **28**, 1150 (1983).